Title

High throughput electrochemically driven metal microprinting with multicapillary droplet cell

Author Names

Muhammad Bilal[1)] and Masatoshi Sakairi[2)]

Affiliations

1) Graduate School of Engineering, Hokkaido University, Kita-13, Nishi-8, Kita-ku, Sapporo, Hokkaido 060-8628, Japan*.

2) Faculty of Engineering, Hokkaido University, Kita-13, Nishi-8, Kita-ku, Sapporo, Hokkaido 060-8628, Japan.

Corresponding Author

*Muhammad Bilal
Graduate School of Engineering,
Hokkaido University
Kita-13, Nishi-8, Kita-Ku, Sapporo, 060-8628, Japan
Tel: +81-11706-7112
Fax: +81-11-706-7881
m-bilal@eis.hokudai.ac.jp
bilal.zafarullah947@gmail.com

***Current Affiliation**

Department of Chemistry, Lehigh University, 6 East Packer Avenue, Bethlehem, Pennsylvania 18015, United States.

mub220@lehigh.edu

Abstract

A high speed and low-cost electrochemical additive manufacturing method for parallel microprinting of metals is proposed. Multicapillary 3D printed solution flow type microdroplet cells (Sf-MDC) with large capillary diameters (600 µm) are used to electrodeposit high-quality Ni microstructures. Three Ni lines each having a width of around 900 µm and a thickness of around 24.6 µm, 20.7 µm and 15.2 µm are simultaneously printed on Cu substrate. The influence of temperature and scanning speed on the height of printed Ni lines is studied. Independent control of solutions inside each capillary enables the simultaneous formation of Ni-Cu-Ni and Cu-Ni-Cu microdots without any cross-mixing of solutions. By replacing 3D printed inner capillaries (around 600 µm in diameter) with silica capillaries (around 100 µm in diameter) inside the Sf-MDC, free standing 3D structures such as Ni microrods are successfully fabricated. Localized electrodeposition using the Sf-MDC allows parallel process 3D printing of metal microstructures for a wide range of applications.

Keywords: Electrodeposition; 3D printing; Droplet cell; Ni microrods; Electrochemistry

1. Introduction

Robust, reproducible and cost-effective fabrication of metals at micrometer scale would enable rapid development of advance electronic devices, microelectromechanical systems (MEMS) and biomedical devices [1–6]. Conventionally, mask-based lithography is the main standard of industries to produce micro- or nano- scale patterns. However, production of expensive masks, time-consuming pre- and post-processing steps and difficulty in fabricating freestanding 3D structures are some limitations of this technique [7,8]. One-step fabrication techniques such as focused ion beam-induced deposition (FIB-ID), electrohydrodynamic printing (EHD), direct ink-writing (DIW), laser induced forward transfer (LIFT), local electrophoretic deposition (EPD), and laser induced photoreduction (LIPR) have also been used to manufacture metal microstructures for various applications [9–13]. Organic material contamination and high carbon content in FIB-ID processes may hinder the properties of printed structures. EHD and DIW methods often need sintering, and removal of binders and solvent, which may result in porous structures and reduce the mechanical strength of the printed metals [14]. Besides the above mentioned techniques, robocasting [15], hybrid metal additive manufacturing [16], metal jetting [17] and laser engineering net shaping [18] techniques have also been utilized for 2D and 3D fabrication of metal microstructures. However, high equipment costs and risk factors associated with the use of high-power lasers and heat treatments limit the use of these techniques.

In recent years, additive manufacturing of metal microstructures using electrochemical microdroplet cells is gaining attention [19–30]. In this technique, micro- or nano-sized capillaries are used for localized electrodeposition of metal ions from the solution. Template free fabrication of complex structures without the use of thermal treatments makes this technique simpler, safer, and cost-effective as compared to previously mentioned techniques. Recently, Chen et al. has reported a low-cost electrochemical metal 3D printer capable of printing highly conductive copper microstructures of 400 µm feature size [31]. Lei et al. has reported a meniscus-confined electrodeposition approach for microprinting of copper lines on gold, silicon and glass-substrates [32]. Lin et al. has also reported a nanopipette based metal microprinting technique capable of fabricating high aspect ratio and high density 3D structures with nanoscale precision [33]. Most of these techniques are limited to micro- or nano- scale resolution and cannot be scaled up. Slow deposition rates (0.008 to 20.4 $\mu m^3 s^{-1}$) and printing speeds (100 to 180 nms^{-1}) are the major challenges to overcome [31]. Research on the fabrication of metal microstructures using large sized nozzles or capillaries is still in its early stages. Technological advances in terms material diversity, high-throughput and large spatial resolution are required for the industrial implementation of electrochemical droplet cell based additive manufacturing.

High-throughput fabrication of metal microstructures can be achieved by combining multiple capillaries in a parallel manner that are capable of simultaneous electrodeposition. The deposition rate or printing speed can be increased by the use of large sized capillaries [34]. Few studies have reported the applications of parallel, multi-capillary 3D printing for fast fabrication of metal microstructures [29, 31–33]. These studies are limited to fabricating metal microstructures in the range of 1-10 µm and offer slow deposition rates. The droplet cells are fabricated manually using a series of complex processes. Problems such as capillary clogging due to small diameter and the need to replace the cell after several hours of usage require fabrication of new cells which consumes time. A single-step method to simultaneously fabricate electrochemical droplet cells with multiple capillaries for high-throughput electrodeposition would be important for a broad range of patterning applications [38].

Herein, a single step fabrication method is applied to fabricate a multicapillary 3D printed solution flow type microdroplet cell (Sf-MDC) with capillary diameters of 600 µm. Unlike manually made droplet cells, multiple Sf-MDC are fabricated at once with minimum resin consumption and shorter fabrication time. An electrochemical additive manufacturing system is developed for the simultaneous electrodeposition of Ni microstrips on Cu substrate. The influence of temperature and scanning speed on the volume of deposit is studied. An attempt is made to simultaneously fabricate three separate Ni, Cu, Ni and Cu, Ni, Cu microdots on the specimen. Free standing Ni microrods are simultaneously fabricated using the Sf-MDC.

2. Experimental

Design and Fabrication of Sf-MDC

Fig. 1 depicts the design and fabrication of Sf-MDC used for simultaneous electrodeposition. Blender 2.79 CAD software was used to design the Sf-MDC. Fig. 1 (a) shows the top view of Sf-MDC. The Sf-MDC consists of three solution inlets capable of separately supplying the solution to the inner capillaries. The type of solution, its flowrate and concentration inside each capillary can be independently controlled. The outer capillaries are used for the continuous removal of excess solution through a common solution outlet. The diameter of inner and outer capillaries is 0.6 mm and 1.2 mm, respectively. Due to the complexity of the design and the limited resolution of 3D printer (Formlabs, Form 2), further decrease in the diameter of capillaries resulted in the blockage of capillary heads inside the Sf-MDC. A photopolymer resin (FLGPCL04, Formlabs Form 2) was used for fabricating the Sf-MDC. Fig. 1 (b) shows the image of 3D printed cells attached to the build platform. Multiple cells can be printed at once using a single-step fabrication method with minimum usage of polymer resin. The single cell consumes only about 5 mL of resin and can be used several times. An important aspect of this technique is its simplicity, high-throughput capability and low-cost, especially when compared with manually made droplet cells and micropipette-based techniques.

Materials

Cu sheets (0.1x10x30 mm) were used as a substrate (working electrode). The sheets were cleaned with ethanol and highly purified water. 0.31 M $NiSO_4 \cdot 6H_2O$/ 0.4 M H_3BO_3 solution was prepared for Ni electrodeposition. 1 M $CuSO_4 \cdot 5H_2O$/ 0.9 M H_2SO_4 was prepared for Cu electrodeposition. The chemicals were purchased from Kanto chemicals, Japan. Pt wires (50 µm in diameter) were inserted inside the inner capillaries of Sf-MDC and connected with a common Pt wire (500 µm in diameter) to use as anode. Cu sheets and Pt wires were purchased from Nilaco Corporation, Japan.

Procedures

Fig. 2 schematically depicts the procedure of simultaneous electrodeposition using the Sf-MDC. The substrate is placed on a computer controlled XYZ moving stage. The inlets of the Sf-MDC are connected with three peristaltic pumps. The solution was supplied to the inner capillaries at a flowrate of 1.5 μm^3 to form droplets at the three capillary tips. The solution droplets were allowed to come in contact with the specimen. Separation distance of around 50 µm was maintained between the specimen and the inner capillary tips. A vacuum pressure of 85 KPa was set to remove the solution from a common outlet with a vacuum pump. Continuous removal of the used solution ensured uniform solution composition at the electrode-electrolyte interface and gave Sf-MDC the ability to control the droplet size by controlling the vacuum pressure. By following these parameters, reproducible meniscus could be formed under each capillary during the metal microprinting process. A constant current of 500 µA is applied to print Ni microstrips and Ni-Cu-Ni microdots on the Cu substrate. The moving speed and temperature of the XYZ stage were varied to examine the influence of these parameters on volume and height of the deposit. Free-standing Ni microrods were simultaneously fabricated by inserting silica capillaries (diameter = 0.1 mm) instead of using 3D printed inner capillaries (diameter = 0.6 mm) to better control the structure of the deposit and prevent the capillary blockage issues. A constant current of 300 µA was applied and the stage was kept stationary for first 30 min of electrodeposition process. The stage was then moved along z-axis at constant speed (0.25 μms^{-1}) to fabricate the microrods.

Observations

The surfaces and cross-sections of the specimens were observed with an optical microscope (Wraycam, NOA630, Tokyo, Japan) and a scanning electron microscope equipped with an energy-dispersive X-ray spectroscopy (EDS) analyzer (SEM, JEOL, JSL6510-LA, Tokyo, Japan). For cross-sectional measurements, the specimens were cut using a cutting machine (RC-120, Ritoku Co. Ltd., Japan) and ultrasonically cleaned with ethanol. The cross-sections of the specimen were embedded inside the epoxy resin and allowed to cure for two days. The exposed surface of the specimens was mechanically abraded with a series of SiC abrasive papers under running water. The abraded specimens were washed with ethanol and highly purified water before SEM observations.

3. Results and discussions

As the electrodeposition process is initiated with Sf-MDC, metal microprinting simultaneously takes place under the droplets-confined microcapillaries. Precise movement of stage in X-, Y- and Z- directions results in fabrication of desired microstructures. This process is similar to fused deposition modeling (FDM) printing process, except the hot end of the extruder filled with melted resin is replaced with droplet-confined microcapillaries, capable of simultaneous electrodeposition. The electrochemical cell (Sf-MDC) enables the control of electrochemical parameters such as current or voltage during the printing process.

Fig. 3 shows the optical, SEM and EDS elemental mapping images of Ni microstrips printed on Cu substrate. The optical microscope image of the specimen (Fig. 3 (a)) shows three uniformly sized Ni lines simultaneously printed on Cu substrate at two different scanning speeds (2 μms^{-1} and 4 μms^{-1}). A slight decrease in the width of lines is observed as the scanning speed is increased from 2 μms^{-1} and 4 μms^{-1}. This may be attributed to the stability in the movement of droplets at higher scanning speeds which allows the droplets to maintain the surface tension equilibrium. The size of the droplets also depends on the wettability and contact time, diameter of inner and outer capillaries and the distance between the specimen and the capillary tips. The height of the printed Ni lines was estimated from the cross-sectional SEM images. The specimen was cut from the middle of fabricated Ni lines. Fig. 3 (b) shows the EDS mapping images of the printed Ni fabricated at 4 μms^{-1}. The deposition rate in the central region is higher than at the edges, resulting in convex shaped cross-sections of the printed Ni lines. This may happen due to higher current density in the central region of the droplets as compared to the edges. The presence of capillary forces and surface tension at the electrode-electrolyte interface allow the droplets to minimize their surface area. Maximum volume of the droplets is thus confined in the central region, resulting in low solution resistance and higher current density. However, very thin layer of droplets spreads outside the diameter of inner capillaries (Fig. S1) and results in high solution resistance. Similar results have been obtained in previous studies [28,32,39]. The shape and height of the simultaneously printed lines are different. Several factors were taken into consideration to investigate the reason of this difference after repeated experiments gave similar results. Since the Sf-MDC is fabricated by stereolithography type 3D printer having a minimum resolution of 100 µm, a slight variation in the dimensional accuracy of capillaries could lead to difference in the IR drop inside each capillary. The use of high-resolution 3D printers capable of accurately fabricating complex designs having multiple micro- or nano-meter sized capillaries may solve this problem. Factors such as variation in solution removal from each inner capillary through a common outer capillary, unequal distance of droplets from the working electrode and irregular distribution of current through the inner capillaries may also lead to a difference in the height of each printed line. In this study, a single power supply was used to supply the current to the three inner capillaries through a common counter electrode as shown in Fig. 2. The use of separate power supplies for each inner capillary may result in uniform supply of current but with added cost. Fig. 3 (c) shows the cross-sectional SEM images of the specimen. The height of the printed lines is around 24.6 µm, 20.7 μm and 15.2 μm, respectively. The volume of each printed line can be calculated by considering the shape of deposit as a trapezium (Fig. S2). The total volume of simultaneously printed lines is around 0.133 mm^3 (1.3×10^8 μm^3). The-deposition rate (printing speed) using this method is around 800 $\mu m^3 s^{-1}$, and width of deposit ranges from 800 μm to 1100 μm. Simultaneous use of three capillaries with large capillary diameters (600 μm) significantly enhanced the printing speed. It is worth mentioning that the highest printing speed previously achieved using the droplet cell or meniscus confined electrodeposition technique ranges from 10^{-3} to 10^2 $\mu m^3 s^{-1}$at feature size of 10^{-1} to 10^2 μm, respectively [5,7].

The influence of temperature and scanning speed on the height of deposit and volume of deposition is shown in Fig. 4. For simplicity, a single capillary is used to deposit Ni line on the substrate. As the temperature of the specimen is varied from 20 °C to 65 °C, the height of deposit increases from 16.5 μm to 27 μm (Fig. 4 (a)). Although the height of deposit is mainly influenced by the applied current (or voltage), increase in temperature may slightly increase the coating thickness due shift in the activation energy of the reaction. This increases the overall reaction kinetics, and more Ni ions are deposited at the cathode [40–42]. However, the quality of electrodeposited lines may start to degrade at higher temperatures due to thermal stresses. Fig. S3 shows the cross-sectional SEM of the electrodeposited lines fabricated at different temperatures. Fig. 4 (b) shows the influence of moving speed on the volume of deposition. As the scanning speed is increased from 2 $\mu m s^{-1}$ to 8 $\mu m s^{-1}$, the deposition volume decreases from around 4.8×10^{-3} mm^3 to 0.9×10^{-3} mm^3. Higher scanning speed leads to a decrease in the volume of deposit due to less contact time between the droplet and the specimen. Fig. 5 shows the ability of Sf-MDC to simultaneously use different electrodeposition solutions during the metal microprinting process. Fig. 5 (a) shows the schematic of Sf-MDC during the Ni-Cu-Ni electrodeposition process. Due to the use of separate pumps for each inner capillary of Sf-MDC, the composition of electrodeposition solution and flowrate can be independently controlled.

Fig. 5 (b) shows the optical microscope image of the Ni-Cu-Ni microdots simultaneously printed on Cu substrate. The diameter of Ni microdots is about 800 µm while the diameter of Cu microdot is about 1000 µm, although all the inner capillaries have same diameter (600 µm). Similar results were obtained in case of Cu-Ni-Cu microprinting (Fig. S4). This may happen because the current efficiency of Cu is higher than the current efficiency of Ni. Since the Cu substrate was used to deposit Cu from $CuSO_4 \cdot H_2SO_4$ solution, some dissolution may happen due to the presence of H_2SO_4 in the solution. Fig. 5 (c) shows the EDS elemental mapping images of Ni-Cu-Ni microdots. Pure Ni and Cu microdots are obtained without any contamination or cross-mixing of solutions. Cu substrate and printed Cu microdot could not be distinguished from the EDS image. The printability of Cu microdot was ex1amined from the CSLM image and height profile of Cu deposit (Fig. S5). The microstructure of deposited Cu is very different from the Cu substrate (Fig. S4). The surface SEM images of simultaneously printed Ni and Cu microdots are shown in Fig. 5 (d). The Ni deposit consists of coarse structure while Cu deposit consists of fine structure. The surface roughness and crystallite size increase by raising the current density [41]. Using Sf-MDC, the optimum applied current is 50-100 µA for Ni electrodeposition and 300 µA for Cu electrodeposition [28]. Since a single power supply was used to supply current to multiple capillaries in this study, a current of 300 µA was set for simultaneous electrodeposition. This resulted in higher surface roughness of Ni. Simultaneous electrodeposition using different solutions can be applied for fabrication of resistance-controlled metal micropatterns for electronics applications.

An attempt was made to fabricate freestanding 3D structures such as Ni microrods by Sf-MDC based parallel metal microprinting process. Fig. 6 illustrates the possibility of fabricating Ni microrods on Cu substrate using 3D printed Sf-MDC and conventional Sf-MDC. Fig. 6 (a) shows that three microrods having different aspect ratios are simultaneously fabricated on the specimen. Large capillary diameters (600 µm) and variation in the dimensional accuracy of capillaries is one reason behind non-uniform fabrication of microrods. The use of high-resolution 3D printers capable of accurately fabricating micro- or nano-meter sized capillaries may solve this problem. Maintaining level build-up of materials under each capillary is another important issue to be addressed. Use of separate power supplies for each capillary may also solve this issue but with increased cost. Synchronizing the withdrawal speed of Sf-MDC with the growth rate of deposit is critical in maintaining the level build-up of materials under the capillaries. Higher withdrawal speed results in a decrease in the diameter of microrods. As the withdrawal speed is increased further, the deposit breaks its contact with the droplet. On the other hand, too slow withdrawal speed results in capillary clogging. Fig. 6 (b) shows that high aspect ratio and high-quality Ni microrod can be fabricated by using conventional Sf-MDC. Use of silica capillaries (diameter = 100 µm) instead of 3D printed capillaries (diameter = 600 µm) results in uniform fabrication of Ni microrod. Optimized withdrawal speed and smaller capillary diameters result in smooth fabrication of 3D structures as compared to large sized capillaries.

Fig. 7 shows the simultaneous fabrication of Ni microrods with modified Sf-MDC. In this case, silica capillaries are used as inner capillaries. The optical microscope image (Fig. 7 (a)) shows the formation of two Ni microrods with different sizes. The formed micro-rods have sufficient strength to support their own weight. Due to the instabilities that occur during the process, one droplet breaks its contact with the microrod while other continues to grow. Fig. 7 (b) shows the SEM images of the fabricated microrods. The microrod-1 has a non-uniform diameter and breaks its contact with the droplet after 2 h. The microrod-2 has a uniform diameter and continues to grow after microrod-1 breaks its contact with the droplet. The magnified view of SEM images shows that the microrods have different morphologies. Because of the variation in solution removal from each inner capillary through a common outer capillary and irregular distribution of current through the inner capillaries, uniform fabrication of equally sized microrods using this technique is still a challenge. This study provides a step forward towards the development of high speed and low-cost metal 3D printers. By properly optimizing the Sf-MDC and changing the designs of capillaries, an array of more complicated 3D metal microstructures than those presented in Fig. 6 and Fig. 7 can be produced with this parallel printing process to significantly multiply the production.

4. Conclusions

3D printed multicapillary solution flow type microdroplet cells are used to successfully develop a parallel, high speed and low-cost electrochemical metal microprinting system. Three Ni lines having uniform width (around 900 μm) and different thickness (around 24.6 μm, 20.7 μm and 15.2 μm, respectively) are simultaneously printed on Cu substrate. The deposition rate or printing speed achieved using this technique is around 800 $\mu m^3 s^{-1}$, and feature size ranges from 800 μm to 1100 μm. An increase in deposition rate is observed at higher temperatures while a decrease in deposition volume is observed at higher scanning speeds. Simultaneous printing of multiple materials (Ni-Cu-Ni and Cu-Ni-Cu microdots) became possible with the Sf-MDC. By using silica capillaries (diameter = 100 μm) as inner capillaries inside the Sf-MDC, two freestanding and straight Ni microrods of different sizes were fabricated. This method can be applied for simultaneous microprinting of resistance-controlled metal microstructures for electronic applications.

Acknowledgements

This study was supported by the Program of the Ministry of Education, Culture, Sports, Science and Technology (MEXT), Japan. SEM observation of this work was conducted at the Laboratory of XPS analysis, Joint-use facilities, Hokkaido University, supported by Material Analysis and Structure Analysis Open Unit (MASAOU).

References

[1] C. Ladd, J.H. So, J. Muth, M.D. Dickey, 3D printing of free standing liquid metal

microstructures, Adv. Mater. 25 (2013) 5081–5085. https://doi.org/10.1002/adma.201301400.

[2] M.A. Skylar-Scott, S. Gunasekaran, J.A. Lewis, Laser-assisted direct ink writing of planar and 3D metal architectures, Proc. Natl. Acad. Sci. U. S. A. 113 (2016) 6137–6142. https://doi.org/10.1073/pnas.1525131113.

[3] M.P. Browne, E. Redondo, M. Pumera, 3D Printing for Electrochemical Energy Applications, Chem. Rev. 120 (2020) 2783–2810. https://doi.org/10.1021/acs.chemrev.9b00783.

[4] A. Ambrosi, M. Pumera, 3D-printing technologies for electrochemical applications, Chem. Soc. Rev. 45 (2016) 2740–2755. https://doi.org/10.1039/c5cs00714c.

[5] I. Liashenko, J. Rosell-Llompart, A. Cabot, Ultrafast 3D printing with submicrometer features using electrostatic jet deflection, Nat. Commun. 11 (2020) 1–9. https://doi.org/10.1038/s41467-020-14557-w.

[6] M. Bilal, M. Sakairi, 3D printed solution flow type microdroplet cell for simultaneous area selective anodizing, J. Adv. Res. (2020). https://doi.org/10.1016/j.jare.2020.06.019.

[7] L. Hirt, A. Reiser, R. Spolenak, T. Zambelli, Additive Manufacturing of Metal Structures at the Micrometer Scale, 1604211 (2017). https://doi.org/10.1002/adma.201604211.

[8] L. Hirt, S. Ihle, Z. Pan, L. Dorwling-carter, A. Reiser, J.M. Wheeler, R. Spolenak, J. Vörös, T. Zambelli, Template-Free 3D Microprinting of Metals Using a Force-Controlled Nanopipette for Layer-by-Layer Electrodeposition, (2016) 2311–2315. https://doi.org/10.1002/adma.201504967.

[9] A. Botman, J.J.L. Mulders, C.W. Hagen, Creating pure nanostructures from electron-beam-induced deposition using purification techniques : a technology, (2009).

https://doi.org/10.1088/0957-4484/20/37/372001.

[10] A. Reiser, M. Lindén, P. Rohner, A. Marchand, H. Galinski, A.S. Sologubenko, J.M. Wheeler, R. Zenobi, D. Poulikakos, R. Spolenak, Multi-metal electrohydrodynamic redox 3D printing at the submicron scale, Nat. Commun. 10 (2019). https://doi.org/10.1038/s41467-019-09827-1.

[11] M. Zenou, A. Sa, Z. Kotler, Laser jetting of femto-liter metal droplets for high resolution 3D printed structures, Nat. Publ. Gr. (2015) 1–10. https://doi.org/10.1038/srep17265.

[12] T. Tanaka, A. Ishikawa, S. Kawata, Two-photon-induced reduction of metal ions for fabricating three-dimensional electrically conductive metallic microstructure, (2006) 7–9. https://doi.org/10.1063/1.2177636.

[13] G. Ercolano, T. Zambelli, C. van Nisselroy, D. Momotenko, J. Vörös, T. Merle, W.W. Koelmans, Multiscale Additive Manufacturing of Metal Microstructures, Adv. Eng. Mater. 22 (2020) 1–8. https://doi.org/10.1002/adem.201900961.

[14] M.E.H. Bhuiyan, A. Behroozfar, S. Daryadel, S. Moreno, S. Morsali, M. Minary-Jolandan, A Hybrid Process for Printing Pure and High Conductivity Nanocrystalline Copper and Nickel on Flexible Polymeric Substrates, Sci. Rep. 9 (2019) 1–10. https://doi.org/10.1038/s41598-019-55640-7.

[15] J.E. Smay, J. Zhou, I. Osendi, K. Cai, B. Roma, M. Belmonte, P. Miranzo, Geometrically Complex Silicon Carbide Structures Fabricated by Robocasting, 2666 (2012) 2660–2666. https://doi.org/10.1111/j.1551-2916.2012.05276.x.

[16] G. Manogharan, R. Wysk, O. Harrysson, R. Aman, AIMS- a Metal Additive-Hybrid Manufacturing System : System Architecture and Attributes, Procedia Manuf. 1 (2015) 273–286. https://doi.org/10.1016/j.promfg.2015.09.021.

[17] L.E. Murr, W.L. Johnson, 3D metal droplet printing development and advanced

materials additive manufacturing, Integr. Med. Res. 6 (2016) 77–89. https://doi.org/10.1016/j.jmrt.2016.11.002.

[18] B. Onuike, B. Heer, A. Bandyopadhyay, Additive manufacturing of Inconel 718 — Copper alloy bimetallic structure using laser engineered net shaping (LENS ™), Addit. Manuf. 21 (2018) 133–140. https://doi.org/10.1016/j.addma.2018.02.007.

[19] A. Ambrosi, R.D. Webster, M. Pumera, Electrochemically driven multi-material 3D-printing, Appl. Mater. Today. 18 (2020) 100530. https://doi.org/10.1016/j.apmt.2019.100530.

[20] S. Daryadel, A. Behroozfar, S.R. Morsali, S. Moreno, M. Baniasadi, J. Bykova, R.A. Bernal, M. Minary-Jolandan, Localized Pulsed Electrodeposition Process for Three-Dimensional Printing of Nanotwinned Metallic Nanostructures, Nano Lett. 18 (2018) 208–214. https://doi.org/10.1021/acs.nanolett.7b03930.

[21] A. Behroozfar, S. Daryadel, S.R. Morsali, S. Moreno, M. Baniasadi, R.A. Bernal, M. Minary-Jolandan, Microscale 3D Printing of Nanotwinned Copper, Adv. Mater. 30 (2018) 1–6. https://doi.org/10.1002/adma.201705107.

[22] A. Reiser, L. Koch, K.A. Dunn, T. Matsuura, F. Iwata, O. Fogel, Z. Kotler, N. Zhou, K. Charipar, A. Piqué, P. Rohner, D. Poulikakos, S. Lee, S.K. Seol, I. Utke, C. van Nisselroy, T. Zambelli, J.M. Wheeler, R. Spolenak, Metals by Micro-Scale Additive Manufacturing: Comparison of Microstructure and Mechanical Properties, Adv. Funct. Mater. 30 (2020) 1–20. https://doi.org/10.1002/adfm.201910491.

[23] A. Behroozfar, M.E. Hossain Bhuiyan, S. Daryadel, D. Edwards, B.J. Rodriguez, M. Minary-Jolandan, Additive printing of pure nanocrystalline nickel thin films using room environment electroplating, Nanotechnology. 31 (2020) 1–10. https://doi.org/10.1088/1361-6528/ab48bc.

[24] X. Zhang, Y. Zhang, Y. Li, Y. Lei, Z. Li, A. Sun, G. Xu, M.-F. Yu, J. Guo, Bipolar

Electrochemistry Regulation for Dynamic Meniscus Confined Electrodeposition of Copper Micro-Structures by a Double-Anode System, J. Electrochem. Soc. 166 (2019) D676–D682. https://doi.org/10.1149/2.1291913jes.

[25] C. Wang, M.E. HOSSAIN BHUIYAN, S. Moreno, M. Minary-Jolandan, Direct-Write Printing Copper-Nickel (Cu/Ni) Alloy with Controlled Composition from a Single Electrolyte using Co-electrodeposition, ACS Appl. Mater. Interfaces. (2020). https://doi.org/10.1021/acsami.0c01100.

[26] X. Chen, X. Liu, M. Ouyang, J. Chen, O. Taiwo, Y. Xia, P.R.N. Childs, N.P. Brandon, B. Wu, Multi-metal 4D printing with a desktop electrochemical 3D printer, Sci. Rep. 9 (2019) 1–9. https://doi.org/10.1038/s41598-019-40774-5.

[27] M. Sakairi, F. Sato, Y. Gotou, K. Fushimi, T. Kikuchi, H. Takahashi, Development of a novel microstructure fabrication method with co-axial dual capillary solution flow type droplet cells and electrochemical deposition, Electrochim. Acta. 54 (2008) 616–622. https://doi.org/10.1016/j.electacta.2008.07.017.

[28] M. SAKAIRI, Y. GOTO, K. FUSHIMI, T. KIKUCHI, H. TAKAHASHI, Fabrication of Cu Micro-rods with Co-axial Dual Capillary Solution Flow Type Droplet Cell and Electrodeposition with the Cell, Electrochemistry. 78 (2010) 118–121. https://doi.org/10.5796/electrochemistry.78.118.

[29] J. Hu, M.F. Yu, Meniscus-confined three-dimensional electrodeposition for direct writing of wire bonds, Science (80-.). 329 (2010) 313–316. https://doi.org/10.1126/science.1190496.

[30] S. Daryadel, A. Behroozfar, M. Minary-Jolandan, Toward Control of Microstructure in Microscale Additive Manufacturing of Copper Using Localized Electrodeposition, Adv. Eng. Mater. 21 (2019). https://doi.org/10.1002/adem.201800946.

[31] X. Chen, X. Liu, P. Childs, N. Brandon, B. Wu, A Low Cost Desktop Electrochemical

Metal 3D Printer, 1700148 (2017) 2–7. https://doi.org/10.1002/admt.201700148.
[32] Y. Lei, X. Zhang, D. Xu, M. Yu, Z. Yi, Z. Li, A. Sun, G. Xu, P. Cui, J. Guo, Dynamic "scanning-Mode" Meniscus Confined Electrodepositing and Micropatterning of Individually Addressable Ultraconductive Copper Line Arrays, J. Phys. Chem. Lett. 9 (2018) 2380–2387. https://doi.org/10.1021/acs.jpclett.8b00636.
[33] Y.P. Lin, Y. Zhang, M.F. Yu, Parallel Process 3D Metal Microprinting, Adv. Mater. Technol. 4 (2019) 1–7. https://doi.org/10.1002/admt.201800393.
[34] A. Ambrosi, R.D. Webster, M. Pumera, Electrochemically driven multi-material 3D-printing, Appl. Mater. Today. 18 (2020) 100530. https://doi.org/10.1016/j.apmt.2019.100530.
[35] M. Chen, H. Lee, J. Yang, Z. Xu, N. Huang, B.P. Chan, J.T. Kim, Parallel, Multi-Material Electrohydrodynamic 3D Nanoprinting, Small. 1906402 (2020) 1–7. https://doi.org/10.1002/smll.201906402.
[36] M. Chen, Z. Xu, J.H. Kim, S.K. Seol, J.T. Kim, Meniscus-on-Demand Parallel 3D Nanoprinting, ACS Nano. 12 (2018) 4172–4177. https://doi.org/10.1021/acsnano.8b00706.
[37] M.A. Skylar-Scott, J. Mueller, C.W. Visser, J.A. Lewis, Voxelated soft matter via multimaterial multinozzle 3D printing, Nature. 575 (2019) 330–335. https://doi.org/10.1038/s41586-019-1736-8.
[38] M. Bilal, M. Sakairi, Fast Fabrication of Localized Porous Alumina Patterns with 3D Printed Microdroplet Cell, J. Electrochem. Soc. 167 (2020) 081501. https://doi.org/10.1149/1945-7111/ab8877.
[39] M. Sakairi, F. Sato, Y. Gotou, K. Fushimi, T. Kikuchi, H. Takahashi, Development of a novel microstructure fabrication method with co-axial dual capillary solution flow type droplet cells and electrochemical deposition, Electrochim. Acta. 54 (2008) 616–

622. https://doi.org/10.1016/J.ELECTACTA.2008.07.017.

[40] S.L. Kuo, The influence of process parameters on the MoS2 content of Ni-MoS2 composite coating by the robust design method, J. Chinese Inst. Eng. Trans. Chinese Inst. Eng. A/Chung-Kuo K. Ch'eng Hsuch K'an. 27 (2004) 243–251. https://doi.org/10.1080/02533839.2004.9670869.

[41] T.D. Golden, Electrodeposition of Composite Materials, 2016. https://doi.org/10.5772/60892.

[42] O. Sadiku-Agboola, E.R. Sadiku, O.I. Ojo, O.L. Akanji, O.F. Biotidara, Influence of Operation parameters on Metal deposition in bright Nickel-plating Process, Port. Electrochim. Acta. 29 (2011) 91–100. https://doi.org/10.4152/pea.201102091.

Captions

Fig.1 Top view of Sf-MDC obtained from CAD software, (a), and image showing multiple Sf-MDC printed at once (b).

Fig.2 Schematic illustration of Ni microprinting using the Sf-MDC.

Fig. 3 Optical microscope image of Ni lines fabricated on Cu substrate, (a), EDS elemental mapping images of the specimen cross-sections showing the size of printed Ni lines, (b), and cross-sectional SEM image of the specimen showing thicknesses of the printed Ni lines, (c).

Fig. 4 Influence of temperature on the height of deposition, (a), and influence of moving speed on volume of deposition, (b).

Fig. 5 Schematic of simultaneous electrodeposition using different solutions, (a), and corresponding optical microscope image, (b), EDS elemental mapping, (c), and SEM images, (d).

Fig. 6 Fabrication of Ni microrods with 3D printed Sf-MDC, (a), and conventional Sf-MDC, (b).

Fig. 7 Electrodeposition with Sf-MDC and the corresponding optical microscope image of specimen, (a), and SEM images of the Ni microrods (b).

Figures

(a)

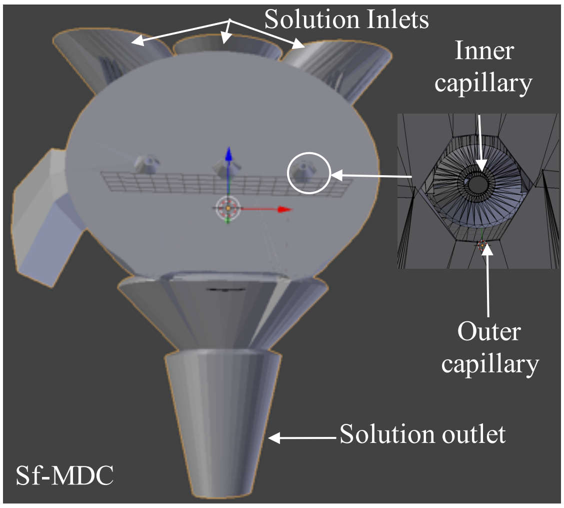

(b)

Fig.1 Top view of Sf-MDC obtained from CAD software, (a), and the image showing multiple Sf-MDC printed at once (b).

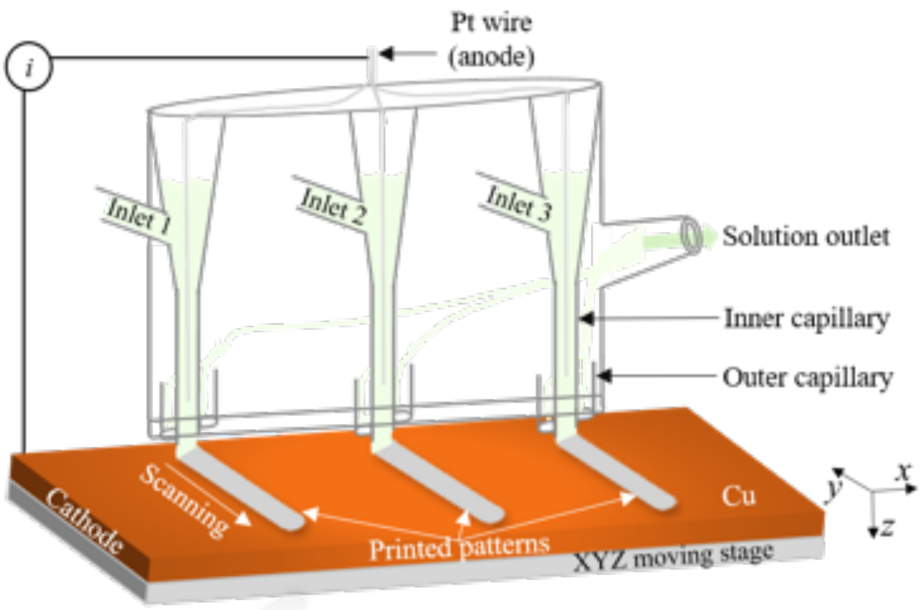

Fig.2 Schematic illustration of Ni microprinting using the Sf-MDC.

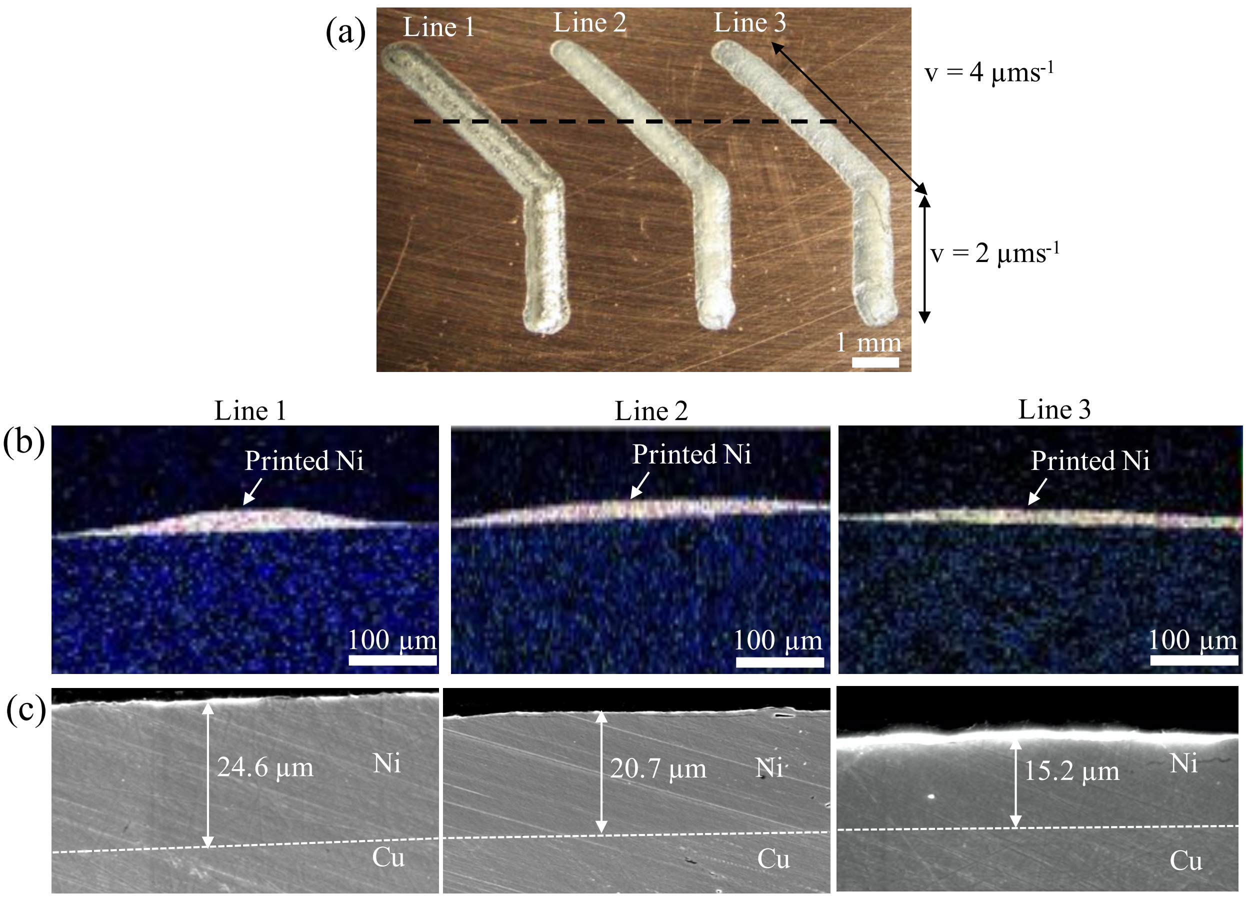

Fig. 3 Optical microscope image of Ni lines fabricated on Cu substrate, (a), EDS elemental mapping images of the specimen cross-sections showing the size of printed Ni lines, (b), and cross-sectional SEM image of the specimen showing thicknesses of the printed Ni lines, (c).

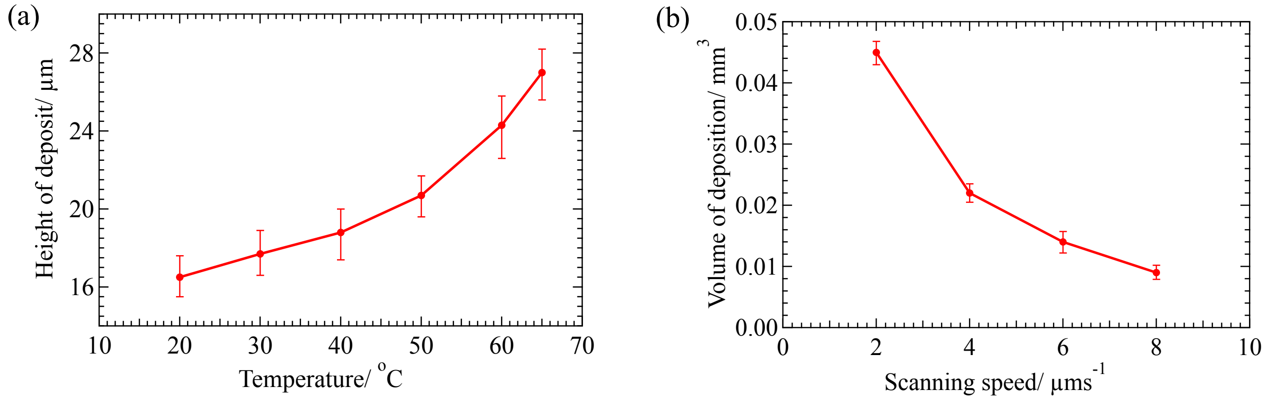

Fig. 4 Influence of temperature on the height of deposit, (a), and influence of moving speed on volume of deposition, (b).

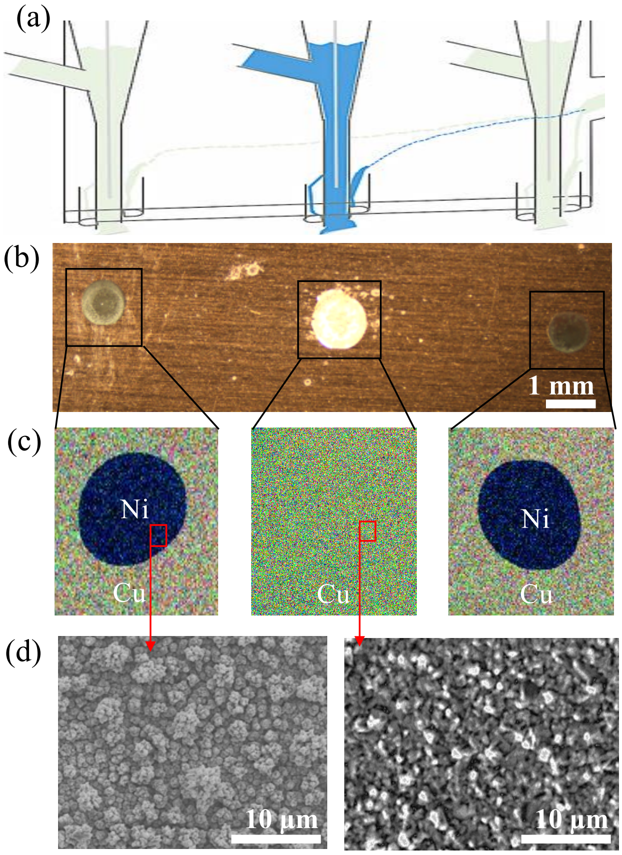

Fig. 5 Schematic of simultaneous electrodeposition using different solutions, (a), and corresponding optical microscope image, (b), EDS elemental mapping, (c), and SEM images, (d).

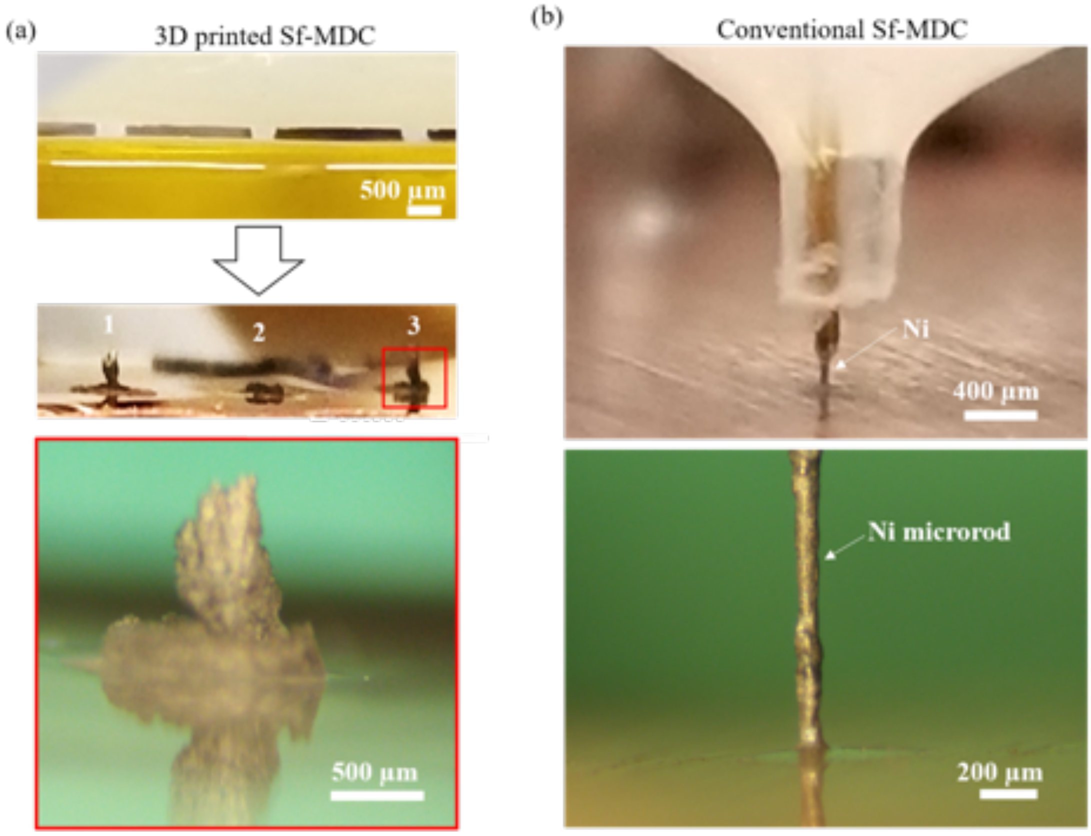

Fig. 6 Fabrication of Ni microrods with 3D printed Sf-MDC, (a), and conventional Sf-MDC, (b).

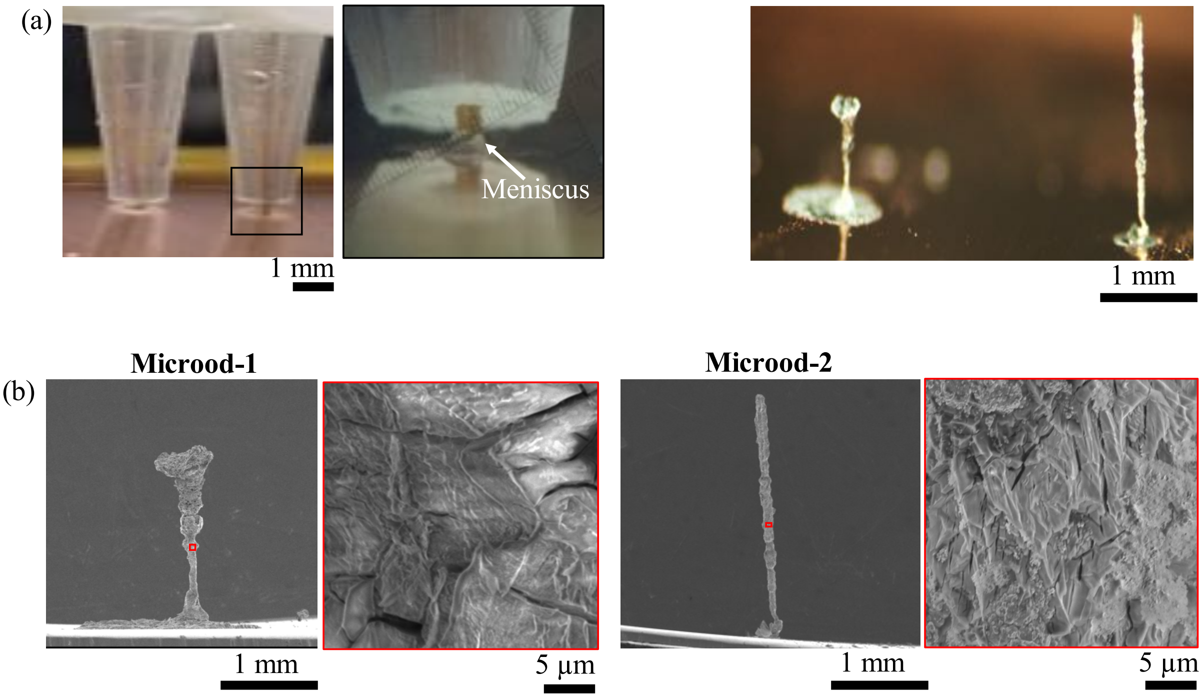

Fig. 7 Electrodeposition with Sf-MDC and the corresponding optical microscope image of specimen, (a), and SEM images of the Ni microrods (b).